JOURNAL OF MATERIALS SCIENCE **35** (2000) 4307–4318

Microstructure and elastic properties of plasma-sprayed alumina

R. J. DAMANI
Department of Structural and Functional Ceramics, University of Leoben, Leoben, Austria
A. WANNER
Institut für Metallkunde, Universität Stuttgart, Stuttgart, Germany

On deposition, plasma-sprayed ceramics are typically far from thermodynamic equilibrium, i.e., they contain metastable phases and also exhibit an extremely high density of lattice and other defects at many microstructural levels. Exposure to high temperatures is known to result in a consolidation of the material and can lead to both subtle and radical changes in the meso and microstructure. The effective elastic properties must be governed by the variety of structural defects and must also change as the defect structure changes during annealing. In the present study the microstructural development in plasma-sprayed alumina (Al_2O_3), as a function of annealing temperature is investigated using techniques of electron microscopy, X-ray diffraction and porosimetry. In addition, the effective elastic properties of this material have been studied using an ultrasonic spectroscopy technique which is especially suited for porous, highly attenuating materials. The results show that annealing even at moderate homologous temperatures already has a noticeable effect on the elastic properties. Upon annealing at higher temperatures, very strong elastic constant changes are observed: increases of about 300% as compared with the as-sprayed material. The underlying microstructural changes are discussed in detail. It is found that the elastic properties of plasma sprayed alumina must be largely governed by the aspect ratio and arrangement of internal defects and porosity.

1. Introduction

Plasma-spraying technology is gaining increasing acceptance in industry for the application of high performance coatings and even for the production of free standing bulk components with up to several millimetres wall thickness [1–3]. The technique is very versatile and almost any material can be plasma-sprayed. For ceramic materials the technique is of particular interest because it allows their application as thermal-barrier and wear resistant coatings on all kinds of standard load-carrying substrates or as highly thermoshock resistant, free-standing parts [4, 5]. The properties of plasma-sprayed ceramics, which are largely governed by their defect-rich microstructures, can, however, be very different from those of corresponding conventionally sintered ceramics. This can be both advantageous and disadvantageous.

Plasma-spraying involves feeding a material powder mixed with a carrier gas/fluid into a high voltage electric arc. The gas forms an expanding plasma, which both melts the powder particles and accelerates them towards a substrate. The molten droplets are deposited at high temperature and velocity on a cooler substrate and are rapidly cooled at rates of about 10^6 to 10^7 Ks^{-1} [6]. Layer thickness is built up by moving the spraying apparatus (Plasma-gun) transversely across the substrate so successive *splats* can be deposited and cooled. After deposition, the plasma-sprayed layer can be separated from the substrate to leave a free-standing ceramic part.

In consequence of the impact and rapid cooling on deposition, a highly aligned, anisotropic microstructure with a high defect density forms, giving rise to peculiar mechanical properties. In particular, the strength and elastic stiffness of a plasma sprayed ceramics are typically an order of magnitude lower than those of the same ceramic when densely sintered [4, 7–9], whereas the fracture toughness can easily be comparable [10]. The unique combination of very low stiffness and decent toughness is responsible for the excellent thermoshock properties of these materials [11].

Post deposition exposure to high temperatures has been observed to lead to significant changes in the phase composition and microstructure of plasma-sprayed ceramics and it has been postulated that these changes must affect the effective elastic stiffness of the material as well as other properties [12]. Several studies on various plasma-sprayed oxide ceramics [3, 13–15], have shown that annealing at elevated temperatures can, indeed, lead to significant residual changes in effective elastic properties: both a decrease and an increase in elastic stiffness has been observed according to the material and annealing schedule. As yet, however, the two features of microstructural and elastic property development have seldom been the subject of a combined comprehensive study on a specific material.

In the present study, we focus on a commercially produced plasma-sprayed aluminium oxide. This material is characterised in as-sprayed state as well as in different heat-treated conditions using X-ray diffraction, electron microscopy and porosimetry. The results of these structural and morphological investigations are correlated with the evolution of the elastic constants of the material, determined by ultrasonic wave velocity measurements.

2. Experimental

2.1. Material and microstructure

The alumina material used in this investigation was atmospheric plasma-sprayed (APS), from an α-Al_2O_3 (99.5%) powder agglomerate, using a water stabilised arc plasma gun, by LWK Plasmakeramik, Gummersbach, Germany. A cylindrical alumina tube was produced with wall thickness of about 80 mm and the substrate was subsequently removed. All samples were cut from the bulk to avoid substrate influence, e.g., substrate/deposit cooling effects. As shown schematically in Fig. 1a and b, the principal material directions are the axial, tangential, and radial directions of the cylinder. In the following, these directions are referred to with the symbols a, t, and r, respectively. The orientation of the splats relative to these directions is shown schematically in Fig 1b. The as-sprayed material contained a mix of about 65% γ and γ-near transition phases and 35% α-Al_2O_3 [10].

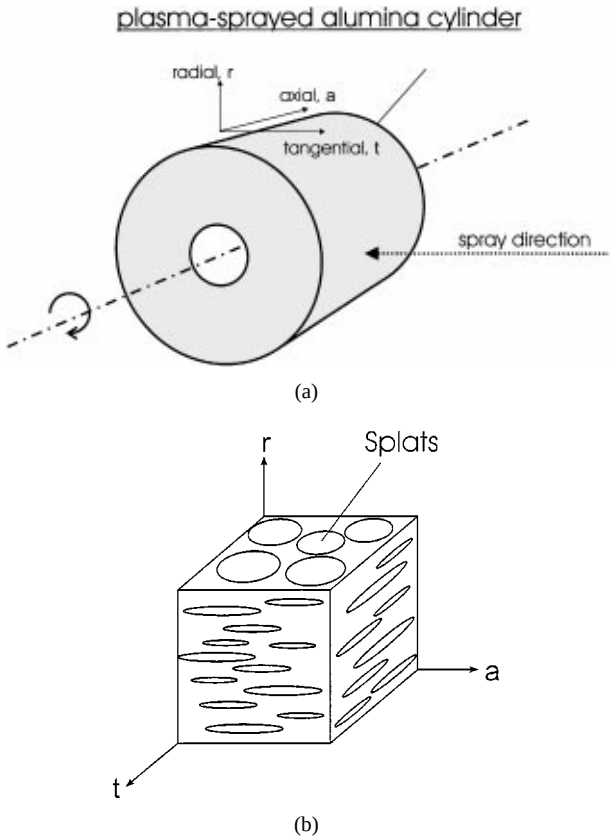

Figure 1 Schematics showing (a) the geometry of the sprayed cylinder and (b) the orientation of the splats with respect to the principal material directions (for simplicity only some splats are outlined, in reality splats impinge on one another).

Samples were heat-treated in air at 5 °C/min with hold times of 12 h at 900 °C, 1050 °C, 1180 °C and 1550 °C, and then furnace cooled to room temperature. These temperatures were chosen on the basis of the known transformation temperatures for the various metastable alumina [16]. The last heat treatment is just below a common sintering temperature for alumina materials [17], and is similar to treatments applied in industry to consolidate and make thermally stable sprayed products.

X-ray phase analysis was conducted using bulk samples and $Cu_{K\alpha}$ radiation in a Siemens D-500 diffractometer. Thin-foil transmission electron microscopy samples were observed and selected area electron diffraction (SAED) studies conducted in a Jeol 2000FX transmission electron microscope (TEM) operating at 200 kV. Scanning electron microscopy (SEM) was conducted on gold sputtered samples in a Leica Cambridge Stereoscan 360. Archimedean porosimetry was used to quantitatively follow the effects of heat treatment and phase change on porosity.

2.2. Characterisation of the elastic stiffness

2.2.1. Ultrasonic measurements

In order to characterize the elastic stiffness, the velocities of elastic waves propagating in the directions of the principal material axes were measured using an ultrasonic spectroscopy technique. For these experiments, cube-shaped samples with nominal dimensions $9 \times 9 \times 9$ mm^3 and edges parallel to the principal material axes a, r, and t were machined from the bulk by cutting and grinding.

Ultrasonic wave velocity measurements were carried out by attaching a pair of identical broadband ultrasonic transducers on opposite sides of the specimen using double sided sticky tape. One transducer was used to transmit a *continuous*, harmonic elastic wave into the specimen, the other one to receive the signal transmitted through the specimen. While sweeping the frequency f of the signal from 100 kHz upwards, the phase shift $\Delta\phi$ between the incident and transmitted waves was measured continuously. It is important to note that there always exists an upper frequency limit above which the attenuation due to scattering and absorption in the specimen is beyond the dynamic range of the measurement system. In the most extreme case of the present study, this upper frequency limit was as low as 2.8 MHz. It is the great advantage of this continuous-wave phase spectroscopy technique over ultrasonic pulse propagation methods that it allows for accurate wave velocity measurements on relatively small samples despite this constraint to relatively low frequencies. A detailed description of the technique and the experimental set-up has been reported elsewhere [18].

The wave velocity, υ, is readily determined from the slope of the resulting $\Delta\phi(f)$ function ("phase spectrum") according to the equation [18, 19].

$$\upsilon = -2\pi L \left(\frac{\mathrm{d}\Delta\phi}{\mathrm{d}f} \right)^{-1}, \qquad (1)$$

in which L is specimen thickness in the direction of wave propagation. Pairs of model V155 and model M110 ultrasonic transducers (obtained from Panametrics Inc., Waltham, MA., USA) were used to measure shear wave and longitudinal wave velocities, respectively. The use of the cube-shaped specimens described above allows for determining nine velocities. These are the three longitudinal velocities υ_{rr}, υ_{aa}, and υ_{tt} as well as the six shear wave velocities υ_{ra}, υ_{rt}, υ_{at}, υ_{ar}, υ_{tr}, and υ_{ta}, where the first index always denotes the direction of wave propagation and second that of the polarization.

The evolution of these velocities after high-temperature annealing was studied by performing measurements on as-sprayed as well as heat treated specimens.

2.2.2. Evaluation

The effective elastic constants of a heterogeneous material are defined as the quantities that relate the average stress σ_{ij} to the average strain ε_{ij} in a representative volume element. The effective elastic behaviour of the material can then be described by the generalised Hooke's law

$$\sigma_{ij} = \sum_{k=1}^{3}\sum_{l=1}^{3} C_{ijkl}\varepsilon_{kl} \tag{2}$$

in which the constants C_{ijkl} are the components of a fourth rank tensor. For simplicity, compact notation is used, i.e. the generalised Hooke's law is written in matrix notation

$$\underline{\sigma} = \boldsymbol{C}\underline{\varepsilon} \tag{3}$$

where C is a 6×6 matrix array of the elastic constants [20].

From the geometry of the manufacturing process, the assumption can be made that the material exhibits at least *orthorhombic* symmetry, corresponding to a stiffness matrix of the form [21]:

$$\boldsymbol{C} = \begin{pmatrix} C_{11} & C_{12} & C_{13} & 0 & 0 & 0 \\ C_{12} & C_{22} & C_{23} & 0 & 0 & 0 \\ C_{13} & C_{23} & C_{33} & 0 & 0 & 0 \\ 0 & 0 & 0 & C_{44} & 0 & 0 \\ 0 & 0 & 0 & 0 & C_{55} & 0 \\ 0 & 0 & 0 & 0 & 0 & C_{66} \end{pmatrix} \tag{4}$$

Hence, nine independent elastic constants are required to fully describe the linear-elastic behaviour of a plasma-sprayed material. We will restrict ourselves to the six constants located on the diagonal of this matrix, which can be obtained from the wave velocity measurements on the cube-shaped samples described above via the following equations:

$$C_{11} = \rho\upsilon_{rr}^2 \tag{5a}$$

$$C_{22} = \rho\upsilon_{tt}^2 \tag{5b}$$

$$C_{33} = \rho\upsilon_{aa}^2 \tag{5c}$$

$$C_{44} = \rho\upsilon_{ta}^2 = \rho\upsilon_{at}^2 \tag{5d}$$

$$C_{55} = \rho\upsilon_{ra}^2 = \rho\upsilon_{ar}^2 \tag{5e}$$

$$C_{66} = \rho\upsilon_{rt}^2 = \rho\upsilon_{tr}^2 \tag{5f}$$

where ρ is the density of the material was determined from mass and dimension measurements performed on the cube-shaped specimens. Equations 5d to f illustrate that the shear wave velocities are pairwise identical ($\upsilon_{ij} = \upsilon_{ji}$). Thus, we expect the measured values of these velocity pairs to be equivalent, which offers the opportunity to test the consistency of the measurement method.

3. Results

3.1. Microstructural and phase development

It is clear from the SEM micrograph of the material cross-section in Fig. 2, that this alumina has the typical layered splat mesostructure expected of plasma-sprayed ceramics. The splats are discontinuously bonded to each other forming very narrow, slit-like inter-splat pores. Other types of more spherical inter and intra-splat pores are also visible. After heat treatment at 1550°C the cross-section of the material looked very similar, with the splat layering largely retained; although it was more difficult to identify the finer splat boundaries and a slight opening of other splat boundaries was also evident.

A summary of the phase development of the alumina system is given in the X-ray diffraction traces in Fig. 3. The transition (metastable) phases increasingly transformed via the intermediate transition phases δ-Al_2O_3 and θ-Al_2O_3 to the thermodynamically stable α-Al_2O_3 with progressively hotter heat treatment. After the heat treatment at 1180°C the transformation to α-Al_2O_3 is almost complete. Material heat treated at 1550 °C was 100% α-Al_2O_3.

Archimedean porosity measurements, summarised in Table I, show the overall porosity remains virtually unchanged up to the reconstructive transformation to α-Al_2O_3. This transformation is accompanied by an increase in porosity of about 4% in absolute terms, despite it requiring a consolidation of material. The heat treatment at 1550 °C reduced the porosity by just over 1% in absolute terms, indicating little overall sintering had taken place.

The splats of the as-sprayed material have an internal, 0.2 to 1 μm wide columnar substructure. An overview of splat substructures is given in the TEM micrograph

TABLE I Summary of changes in porosity levels with heat treatments

	Material Condition/Heat Treatment Temperature				
Porosity, %	As-Sprayed	900 °C	1050 °C	1180 °C	1550 °C
Open	12.6	12.8	13.0	14.6	14.4
Closed	0.7	0.6	0.2	2.7	1.8
Total	13.3	13.4	13.2	17.3	16.2

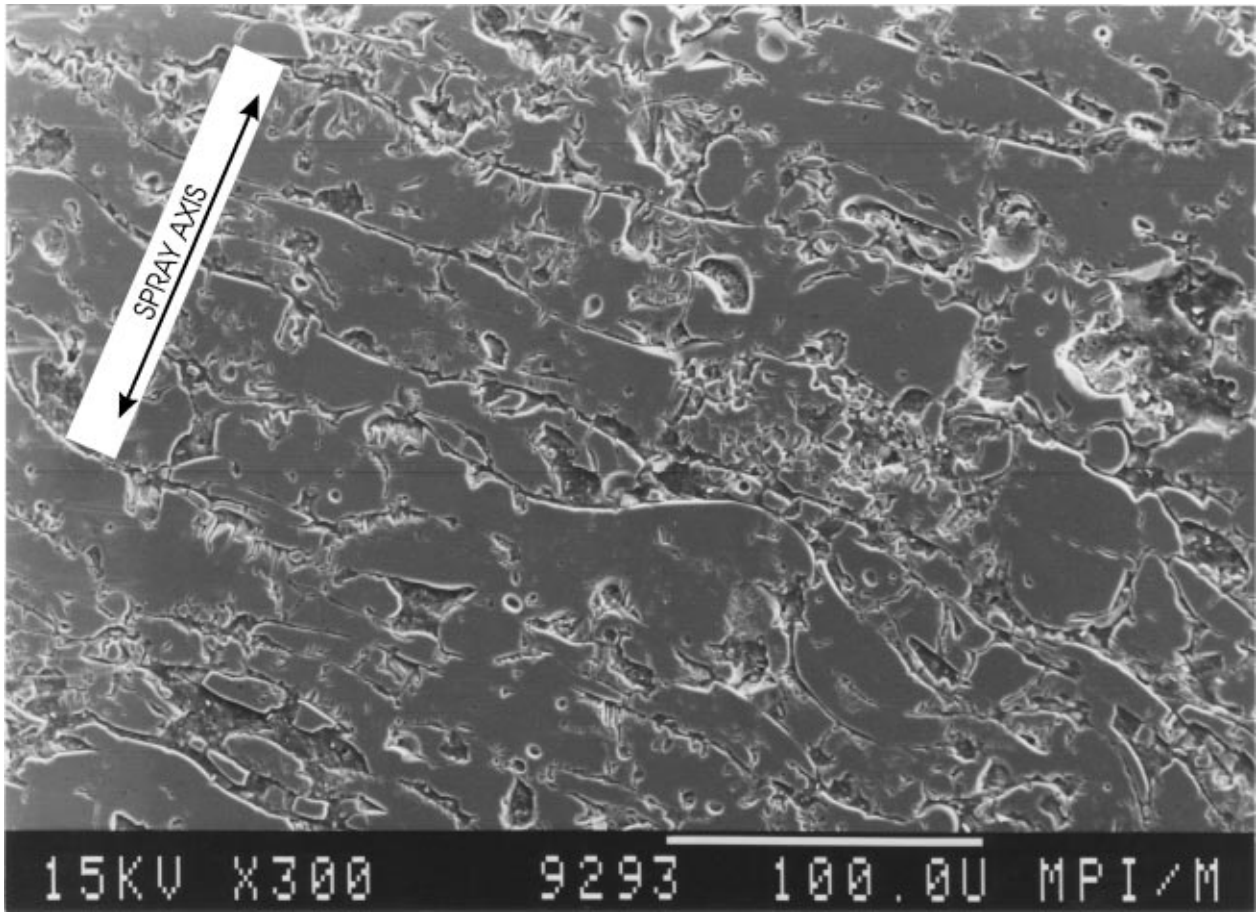

Figure 2 SEM micrograph showing the layered splat microstructure of the as-sprayed material.

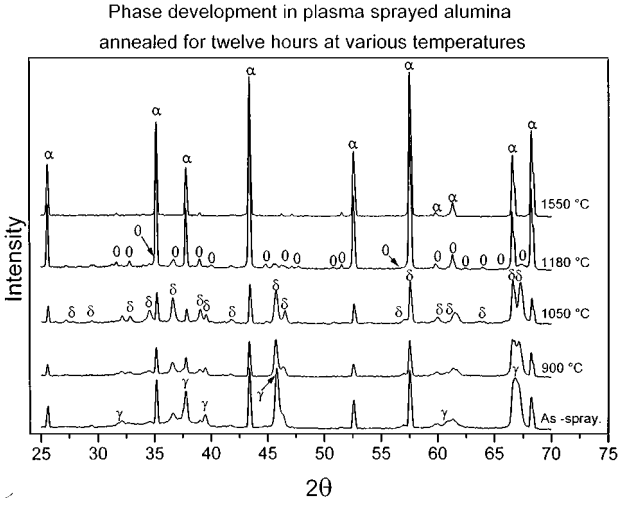

Figure 3 X-ray diffraction traces showing phase development with heat treatment.

shown in Fig. 4a. Cracking between columns can be seen. Agglomeration of porosity was observed at the columnar interfaces. In Fig. 4b a SAED pattern showing the [100] zone axis of γ-Al_2O_3, typical for a single columnar grain is presented. No large degree of ordering is evident in this state. Generally, the as-sprayed material contains a high concentration of internal defects.

TEM observation of the microstructure after annealing at 900 and 1050 °C for 12 h revealed no dramatic overall change from the as-sprayed condition and the intra-splat columnar structure was maintained. However, intra-columnar porosity became more pronounced as pores appeared to precipitate at both existing free surfaces and also in the bulk of the material. This porosity was often very fine and precipitated pores typically had diameters between 10 and 50 nm. The development of such porosity within a single column in material heat treated at 900°C is shown in Fig. 5a. SAED analyses of such columnar grains showed the development of extensive ordering already during heat treatment at 900°C. The SAED pattern in Fig. 5b, showing the [100] δ-Al_2O_3 zone axis, proves that the material has undergone a transformation to this ordered phase. The extent of ordering was seen to increase with the heat treatment at 1050°C.

After twelve hours at 1180 °C the material consists almost completely of α-Al_2O_3. Internally, a structure of laths reminiscent of the original columnar structure has developed (Fig. 6). The amount of intra-splat porosity has visibly increased. Due to the narrow field of view covered by TEM it is not possible to make a definitive evaluation of inter-splat porosity. After 12 h at 1550 °C (Fig. 7) the material consists entirely of α-Al_2O_3. The intra-splat columnar and lath-like substructures have been completely replaced by slightly elongated, randomly oriented grains. Inside the splats, the material is reminiscent of a standard sintered Al_2O_3. Mesoscopically, however, the basic quasi-laminated splat structure still prevails.

A more detailed and comprehensive description of microstructural development with heat treatment in the sprcific material of this study may be found in [12].

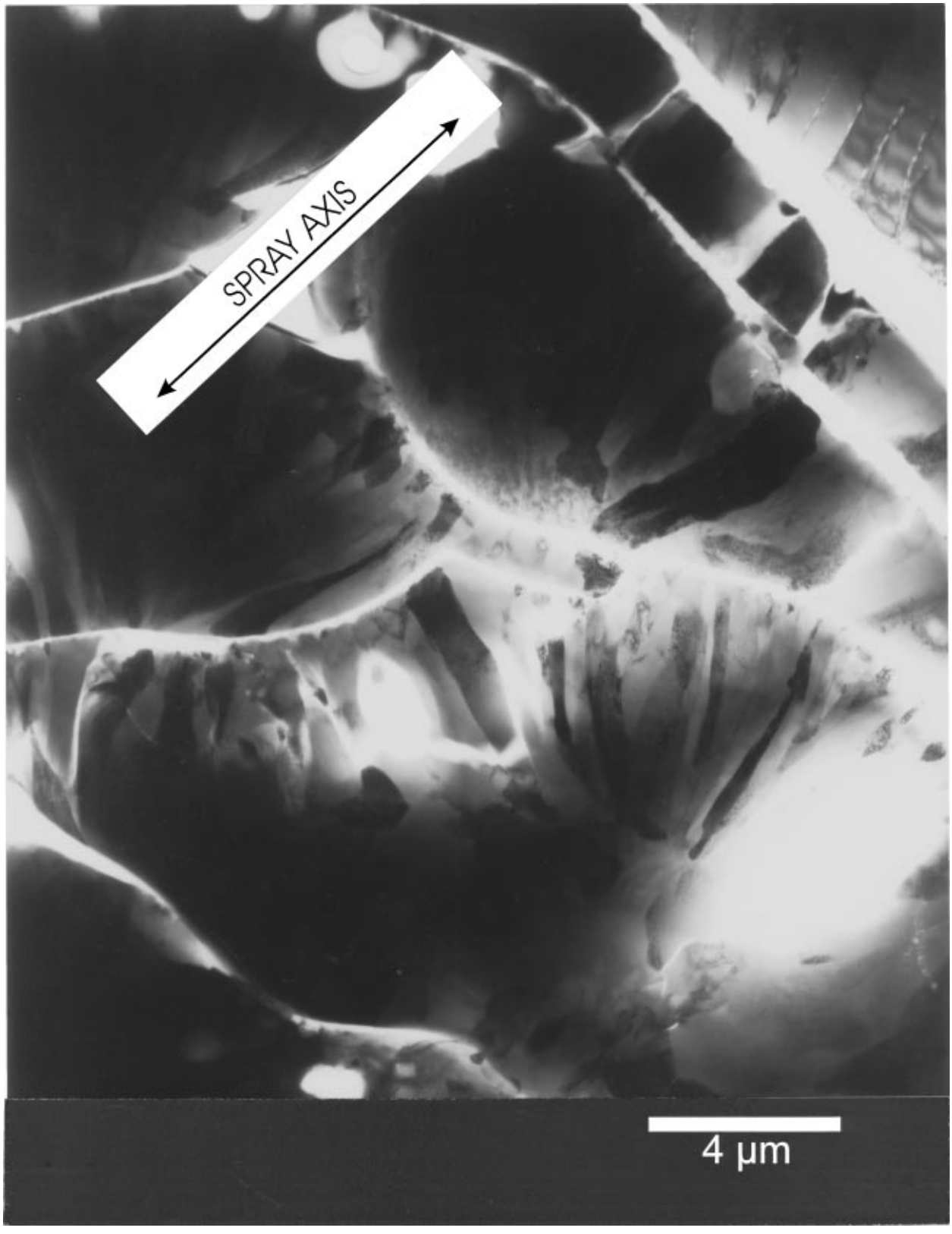

(a)

Figure 4 (a) TEM micrograph of as-sprayed splats exhibiting the internal columnar structure (b) an SAED pattern from one of the columnar grains showing the [100] γ-Al_2O_3 zone axis and little ordering.

3.2. Evolution of elastic properties

In Fig. 8a and b the longitudinal and shear wave velocities, respectively, are plotted against the heat treatment temperature. It can be seen that in all cases the fundamental condition $\upsilon_{ij} = \upsilon_{ji}$ is fulfilled within the error of measurement. Moreover, it appears that the material is transversely isotropic (with isotropy in the t-a-plane, which is the plane perpendicular to the spraying direction), as there is no significant difference between υ_{tr} $(=\upsilon_{rt})$ and υ_{ar} $(=\upsilon_{ra})$ and also no difference between υ_{tt} and υ_{aa}. Hence, the total number of independent elastic constants reduces from nine to five, four of

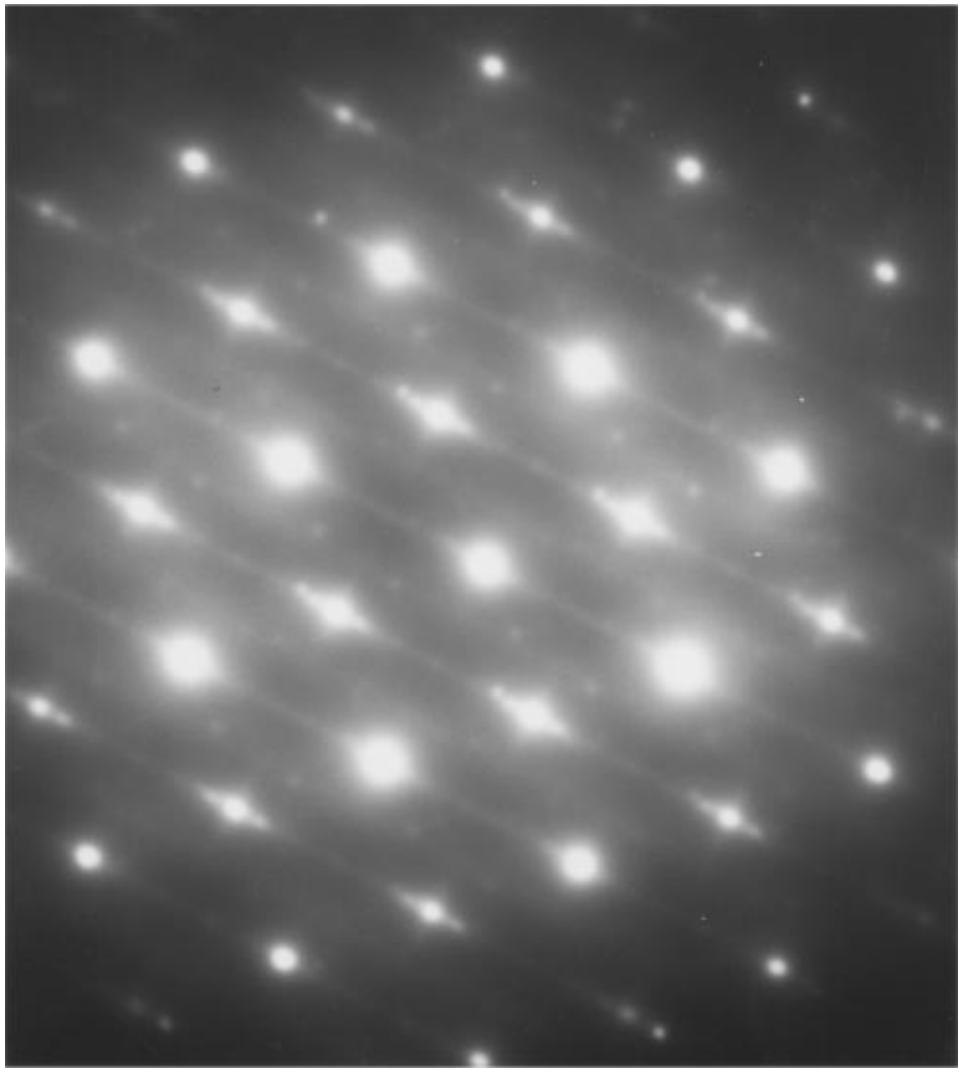

(b)

Figure 4 (*Continued*).

which (C_{11}, $C_{22} = C_{33}$, C_{44}, $C_{55} = C_{66}$) can be determined from these measurements. In Fig. 9a and b these elastic constants are plotted as a function of annealing temperature in logarithmic-linear fashion.

In as-sprayed condition, C_{11} is considerably lower than the C_{22} and C_{33}, i.e., the material is less stiff when uniaxially strained in the direction perpendicular to the splats than when strained in any direction parallel to them. Comparison of the constants C_{44}, C_{55} and C_{66} shows that the resistance of the material against shear in the *t*-*a* plane is greater than in any plane that is parallel to the *r*-direction.

The effect of heat treatment on the stiffness can be divided into two regimes. For the annealing temperatures below 1180°C, a slight but still significant decrease of all elastic constants with increasing annealing temperature is observed. On heat treating the materials at temperatures of 1180°C and above, however, the stiffness increases steeply. Because of the limited number of data points the exact transition between the two regimes cannot be exactly delineated.

In a fully isotropic material the elastic constants C_{11}, C_{22} and C_{33} are equal, and so are the constants C_{44}, C_{55} and C_{66}. The experimentally determined ratios C_{22}/C_{11} (or C_{33}/C_{11}) and C_{44}/C_{55} (or C_{44}/C_{66}) can therefore be used as measures for the degree of anisotropy. (Strictly speaking, the above ratios being equal to 1 alone is not sufficient proof of isotropy, since, for instance, this condition is fulfilled also in the case of an anisotropic material with cubic symmetry. However, since the material studied here exhibits a lower than cubic symmetry in the as sprayed condition, these ratios give a good indication of the evolution towards, or away from, isotropy.) Due to the logarithmic scaling of the stiffness axes in figures 9a and b, the distances between the data points for C_{11} and C_{22} (or C_{33}) in the diagrams are a measure of the deviation of these ratios from unity. The evolution of these ratios is shown explicitly in Fig. 9c. It can be clearly seen that, in the high-temperature regime, the corresponding data trends converge, indicating that the material not only becomes stiffer but also becomes increasingly isotropic.

4. Discussion

It is clear from the structural investigation that the as-sprayed alumina is far from being an equilibrium material. In the as-sprayed state there is a super saturation of both inter and intra-splat defects, providing high driving forces that result in considerable morphological

(a)

Figure 5 (a) TEM micrograph of intra-splat columns in material heat treated at 900°C showing the evolution of microporosity (b) SAED pattern from the central column in (a) showing the [100] zone axis of δ-Al_2O_3 and extensive ordering.

development within splats during heat treatment even at moderate homologous temperatures. In particular, the crack and pore structure of the material evolve significantly during heat treatment, with many aligned cracks healing, others being formed with different spatial arrangement. High temperature heat treatments in particular lead to the precipitation of considerable amounts of intra-splat porosity and the opening of existing pores. Although the heat treatments applied led to significant intra-splat changes, the accompanying inter-splat morphological change was more subtle and little superficial difference could be seen between the mesostructures (splat level) of the as-sprayed and heat treated material. This notwithstanding, the heat treatments cause significant change in its elastic behaviour. Despite the high attenuation caused by the microstructure, the ultrasonic technique used delivered good and reproducible results for the velocity measurements, and it has been possible to successfully follow the evolution of the elastic stiffness of all the material conditions.

The as-sprayed plasma-sprayed material exhibits exceptionally low stiffness compared to densely sintered conventional polycrystalline alumina (for which room temperature Young's moduli typically in the range of 350–400 GPa are reported, e.g., [17, 22]). In the radial direction, the relative stiffness, i.e., the ratio of the effective elastic constant of the plasma-sprayed material to the corresponding constant of the fully dense material is as low as $\sim$0.04, while a rough estimate based on the measured total porosity using standard models developed for conventionally sintered materials [23–25], would predict a relative stiffness of $\sim$0.75. This is obviously a consequence of the splat-based microstructure that includes highly non-spherical pores

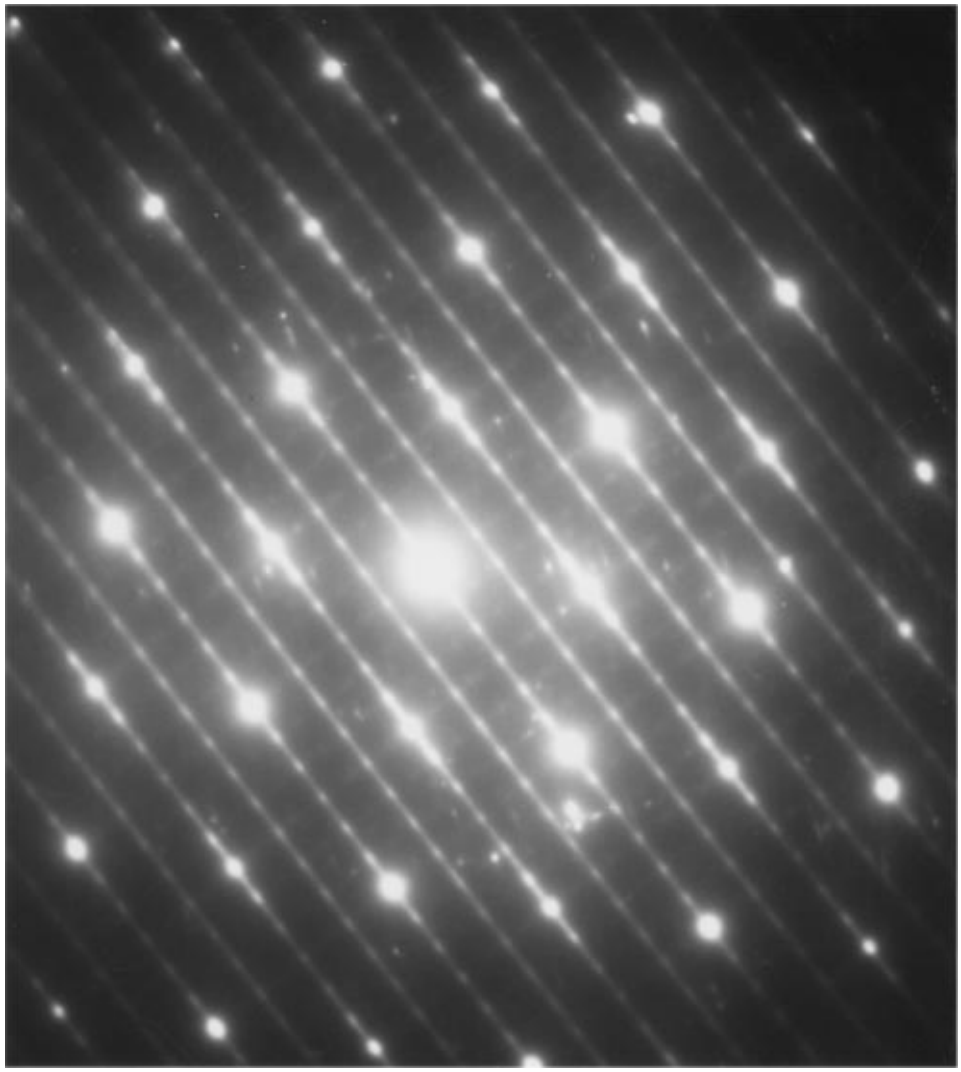

(b)

Figure 5 (*Continued*).

with a high aspect ratio. Since these slit-like pores are preferentially oriented in the *t*-*a*-plane, this also explains the high anisotropy of the material. (Note, C_{11} of polycrystalline α-Al_2O_3 is assumed here to take the value 448 GPa, as estimated on the basis of a Young's modulus of $E = 380$ GPa and Poisson's ratio $\nu = 0.27$; however, even if the Young's modulus was estimated at $E = 300$ GPa, which may be more suitable for γ-Al_2O_3 [26], the relative stiffness would still only take a value about 0.05, which hardly changes the argument.)

The extremely low relative stiffness observed in tangential and axial directions is probably a consequence of two features: (1) the inter-splat slit-like pores are in fact not ideally aligned, and (2), as evident from the TEM observations, the spats themselves are not fully dense and contain agglomerations of pores and microcracks, which are preferentially oriented perpendicular to the splat plane.

Interestingly, in a relatively recent investigation of the elastic constants of a free-standing plasma-sprayed alumina (also using an ultrasonic measurement technique), Parthasarathi *et al*. [27] found the material also to be transversely isotropic, but the elastic constants were significantly higher than those determined in this work ($C_{11} \sim 130$ GPa and $C_{22} = C_{33} \sim 90$ GPa). More importantly, however, it was found that the anisotropy was inverse to that determined here. As the authors, however, provided no microstructural or porosity evidence, it is possible only to speculate that the material of their study was deposited under significantly different conditions, probably leading to better bonding between adjacent splats so that transverse cracking caused by thermal stresses dominated.

After heat treatments at the relatively low temperatures of 900 °C and 1050°C, before the reconstructive phase change to α-Al_2O_3, there is surprisingly, a slight decrease in stiffness. In fact, a similar and even more pronounced drop in stiffness at relatively low homologous temperatures has been previously observed on annealed plasma-sprayed Al-Mg-spinell [14]. Unfortunately, in that investigation there was insufficient microstructural evidence for the author to be able to forward possible mechanisms in detail. However, the author did suggest that annealing at moderate homologous temperatures might cause local fracture at inter-splat bonds due to small shape changes of the splats as recovery processes are activated.

In the present study, the microstructural investigation allows the postulation that such processes are indeed active in alumina, and that the observed drop can be

Figure 6 TEM micrograph of a splat in material heat treated at 1180°C, showing lath-like grains after transformation to α-Al_2O_3 and increased intra-splat porosity.

explained by two effects: (1) the increase in volume of porosity in the splats, as observed by TEM, concurrent with dehydroxylation, ordering and recovery processes, leading to a reduction in the inherent stiffness of splats—such mechanisms have been observed previously in plasma sprayed ceramics, [12, 28]; and (2) perhaps more importantly, by an effective increase in the aspect ratio of inter-splat pores, especially the slit like pores, caused by the precipitation of vacancies at existing pore edges and by the fracture of some inter-splat ligaments. These fractures may occur in consequence of any of the mechanisms listed in (1), as these may cause local splat shape changes, but additionally fracture may also result from thermal expansion mismatch between adjacent splats.

In the high-temperature regime, upon the diffusionally driven reconstructive phase transformation to α-Al_2O_3, two apparently contradictory effects are observed: both relative stiffness and porosity simultaneously, markedly increase. Annealing at 1180°C results in a relative increase in porosity by ∼30%, while, in the radial direction, relative stiffness increases from ∼0.025 to ∼0.06. The increase in porosity with high temperature heat treatment in this material, despite being contrary to expectation, has previously been observed and explained in [12]. In summary, the porosity is thought to develop in consequence of the restrictions in volume contraction imposed by impinging splats during the reconstructive phase transformation. This increase in porosity gives rise to the question why there is no related reduction in stiffness, but rather the opposite, viz., an increase in stiffness occurs.

Although the fact that γ-Al_2O_3 has intrinsically a lower elastic stiffness than α-Al_2O_3 goes some way to explaining the low initial stiffness of the plasma-sprayed alumina and the subsequent stiffness increase

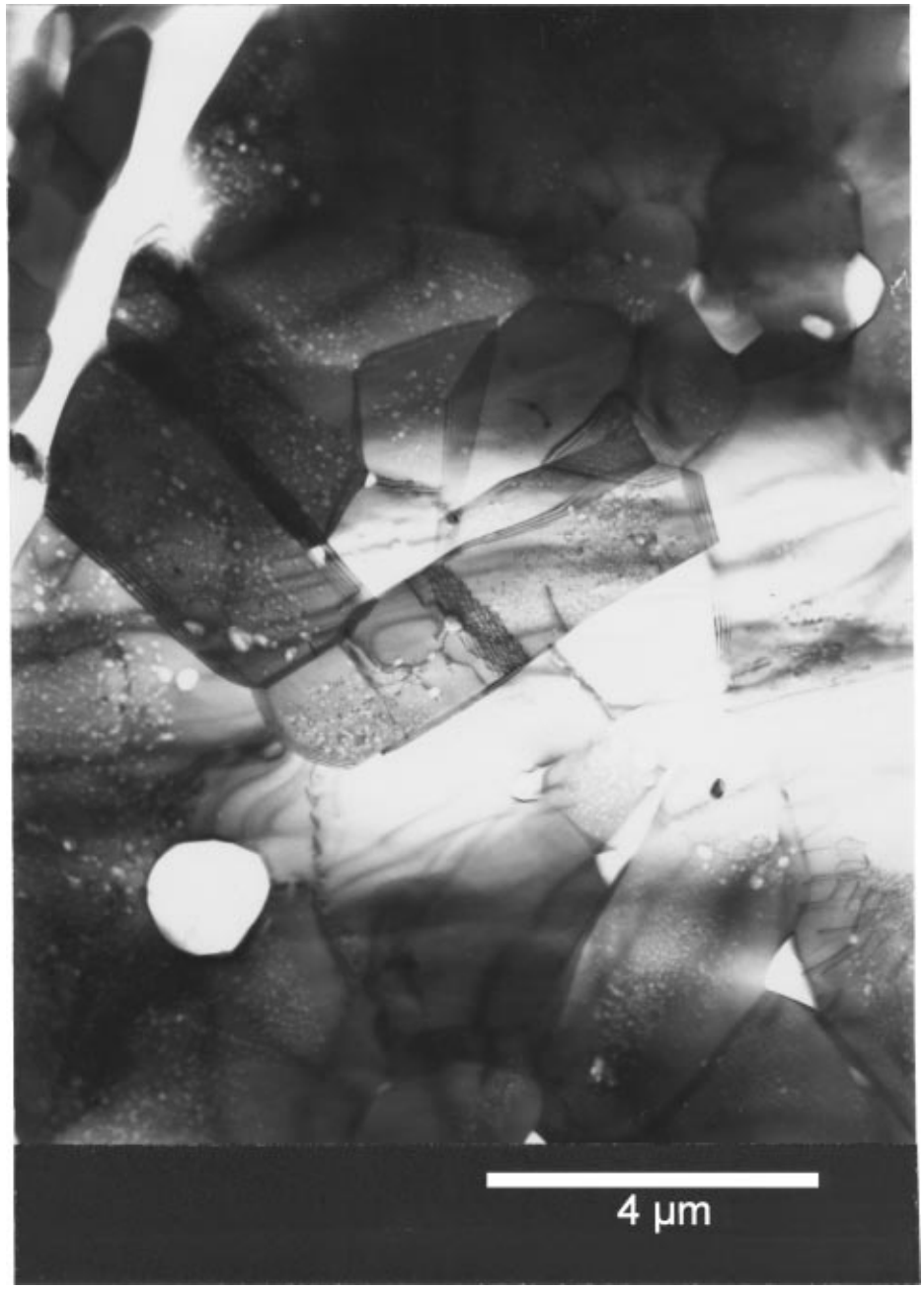

Figure 7 TEM micrograph of a splat in material heat treated at 1550°C, showing recrystallised α-Al_2O_3 grains.

on heat treatment, the difference is not great enough to explain the magnitude of the change observed. From a mechanics aspect, the most suitable and appropriate explanation for such a dramatic increase in stiffness whilst maintaining or increasing the amount of porosity, is if the shapes of the pores change. As shown, e.g., by Kachanov *et al*. [29], for elliptical pores, the reduction in stiffness depends strongly on the aspect ratio, and the closer the pores approach spherical shape, the stiffer the material is. It has also been shown for the case of aligned elliptical pores that this stiffness increase goes along with a reduction of anisotropy.

A very effective way to reduce the aspect ratios of the inter-splat pores is the formation of contact ligaments between previously open interfaces. To illustrate this it is helpful to consider a slit-like pore in a two-dimensional body. The formation of a ligament connecting the opposite faces of the pore in the centre would result in the formation of two pores with half the original aspect ratio, the combined volume of which, however, is almost unchanged from that of the original single pore. Obviously the situation in a real three-dimensional material is more complicated, but it nevertheless follows similar principles. Hence, the formation of very few additional ligaments is required to increase the stiffness considerably. This implies, however, that a significant change in the microstructure is not necessarily observed. That explains why when the microstructure of this material is observed superficially (e.g., in the SEM), it appears to be largely unchanged from the as-sprayed state. Large-scale sintering is not required.

The consolidation of the intra-splat structure observed by TEM may also play a role in increasing the macroscopic stiffness of the material, especially in the tangential-axial plane, where the reconstructive phase change results in an increase in relative stiffness from $\sim$0.09 to $\sim$0.22, which corresponds to a much greater

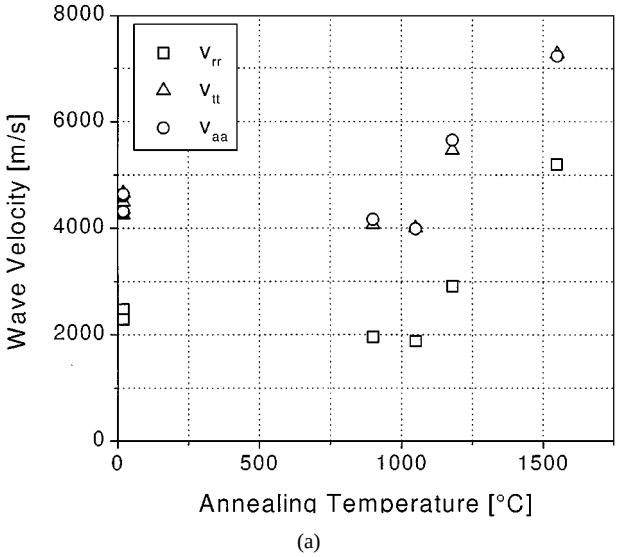

(a)

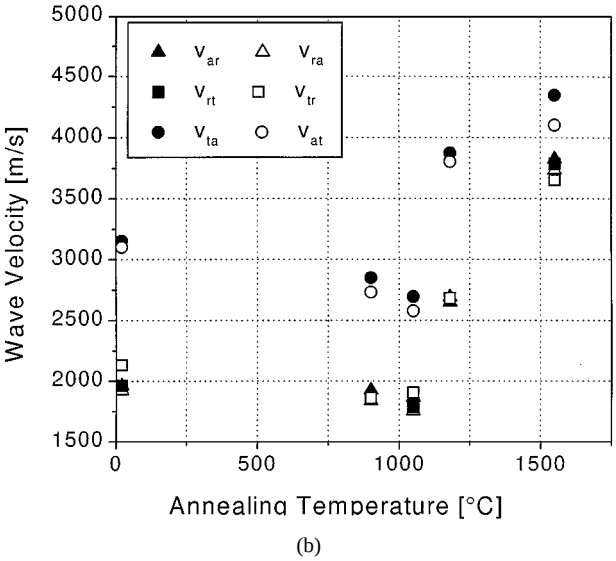

(b)

Figure 8 Graphs of ultrasonic wave velocities as a function of annealing temperature (a) longitudinal waves, (b) shear waves.

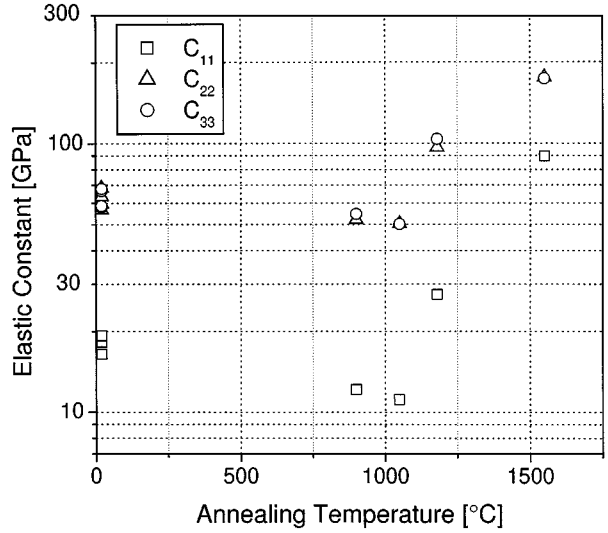

(a)

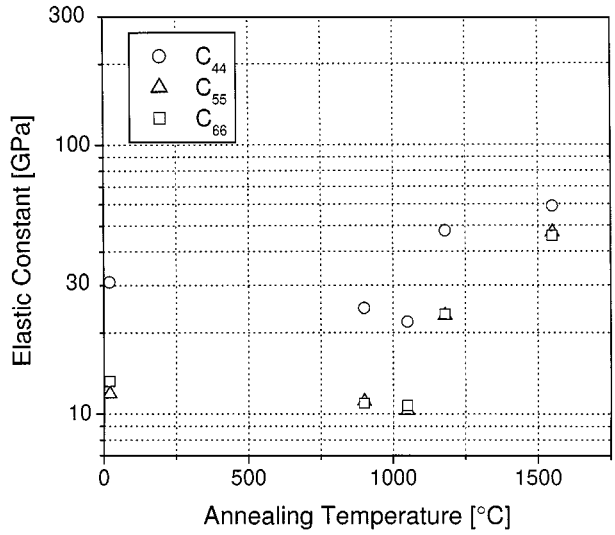

(b)

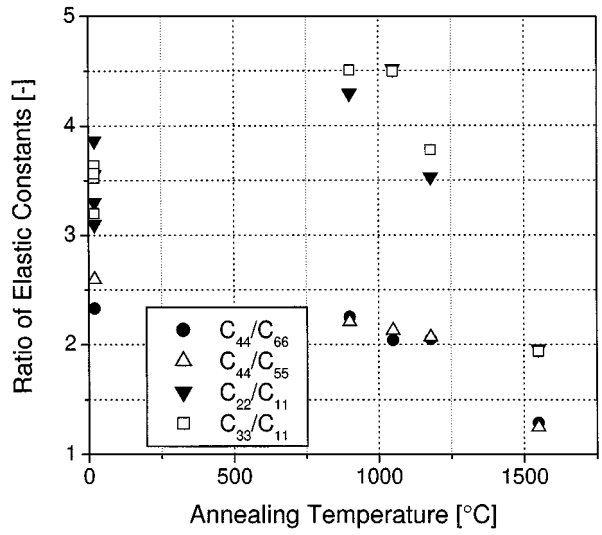

(c)

Figure 9 Graphs of the evolution of elastic constants with annealing temperature: (a) uniaxial-strain constants C_{11} and $C_{22} = C_{33}$, (b) shear constants C_{44} and $C_{55} = C_{66}$, (c) ratios of stiffness showing evolution of anisotropy with heat treatment. Note graphs (a) and (b) are plotted on log-linear axes.

absolute increase than in the radial direction. This is possibly a consequence of the removal of cracks and the more even spatial distribution of the porosity, which effectively makes the splats themselves stiffer.

A third factor that should be taken into consideration is that the precipitation of additional porosity should lead to a reduction in the stiffness of the splats, whereas the transformation of the transition aluminas the α-phase should result in a stiffness increase. These two effects will obviously work against each other, but within the limited scope of this study it is not possible to make an quantitative evaluation of their relative effectiveness. It is certain, however, that the combined effect of these two intra-splat phenomena does not dominate the macroscopic behaviour of the material.

It is evident that this plasma sprayed alumina undergoes complex changes in its pore structure with heat treatment and it is this structure that obviously dominates the materials elastic properties. However, it appears that the form, shape and distribution of the pores plays a more determining role than the actual absolute volume of porosity. Hence it is advisable to exercise

caution when attempting to interpret physical or morphological data and extrapolate to other properties or quantities using the standard and common models of property/porosity dependence. These have usually been constructed for materials with non-interacting, spherical porosity and can lead to gross error in the extrapolated values.

5. Summary and conclusions

- Heat treatment of plasma-sprayed alumina allows the highly non-equilibrium phase composition and microstructure to undergo radical changes towards equilibrium even at moderate temperatures. Defects are consolidated and porosity is precipitated, undergoes metamorphosis and is rearranged. The mesoscopic splat structure, however, is largely maintained.
- Despite the highly attenuating nature of the material, the ultrasonic spectroscopy method applied delivered reliable values of wave velocity, from which the elastic constants could be determined.
- The materials shows two stages of response to heat treatment. At lower temperatures the as-sprayed gamma phase is seen to undergo an ordering transformation to the other metastable allotropes delta and theta alumina. This is concurrent with a slight but real drop in stiffness, which we attribute to elongation of slit-like intersplat pores due to processes of recovery. At higher homologous temperatures a stiffness increase of up to three times the original value and a profound reduction in anisotropy has been achieved, despite an observed increase in porosity. This results from a change in pore morphology (aspect ratio) towards more spherical. Macroscopic sintering, however, did not occur in the temperature range covered by this study.
- The change of intra-splat microstructure certainly contributes to the changes of macroscopic elastic response. However, the changes in effective aspect ratio of inter-splat porosity due to the formation of even a few additional ligaments between adjacent splats can have a much stronger and dominating effect on the stiffness.

Acknowledgements

This work was partially funded by the Austrian Ministry for Science and Transport under contract no. GZ 140.539/3-V/A/6/98. The authors are grateful to Dr. Ekkehard H. Lutz (formerly with LWK Plasmakeramik, Gummersbach, Germany) for providing material and Mr. Martin Selten, Universität Stuttgart, for technical assistance with the ultrasonic measurements. Also gratefully acknowledged for their help with the TEM investigation are Peter Makroczy of the Dept. of Materials Science, Technical University of Košice, Slovak Republic, and Dr. Warbichler and Dr. Hofer of the Forschungsinstitut für Elektronenmikroskopie of the Technical University, Graz, Austria.

References

1. R. W. SMITH, *Powder Metallurgy International* **25** (1993) 78.
2. H. ESCHNAUER and E. LUGSCHEIDER, *Metall* **45** (1991) 458.
3. E. H. LUTZ, plasmakeramik – in *Technische Keramische Werkstoffe*, J. Kriegesmann (Hrsg.), Deutscher Wirtschaftsdienst, Köln (1993), Kap. 3.4.9.1.
4. L. PAWLOWSKI, "The Science and Engineering of Thermal Spray Coatings," (Wiley, 1995).
5. E. H. LUTZ, *J. Am. Ceram. Soc.* **77** (1994) 1274.
6. R. B. HEIMANN, "Plasma-Spray Coating: Principles and Applications" (VCH, Weinheim, NewYork, 1996).
7. R. MCPHERSON, *Surface Coatings and Technology* **39/40** (1989) 173.
8. R. MCPHERSON and P. CHEANG, "Elastic Anisotropy of APS Alumina Coatings and its Relationship to Microstructure, High Performance Ceramic Films and Coatings," Vol. 67, edited by P. Vincenzini, in *Mat. Sci. Monographs* (1991) 277.
9. C. LI, A. OHMORI and R. MCPHERSON, *J. Mat. Sci.* **32** (1997) 997.
10. R. J. DAMANI and E. H. LUTZ, *J. Eur. Ceram. Soc.* **17** (1997) 1351.
11. G. A. SCHNEIDER, R. DANZER and G. PETZOW, *Fortschrittsberichte der DKG* **3** (1988) 59.
12. R. J. DAMANI and P. MAKROCZY, *J. Eur. Ceram. Soc.* **20** (2000) 867.
13. A. WANNER and E. H. LUTZ, *J. Am. Ceram. Soc.* **81** (1998) 2706.
14. A. WANNER, *Mat. Res. Soc., Symp. Proc.* **521** (1998) 45.
15. C. GAULT, S. BOILEVIN and G. DESPLANCHES, *Science of Ceramics* **14** (1988) 389.
16. K. WEFERS and C. MISRA, Oxides and Hydroxides of Aluminium, Alcoa Technical Paper No. 19, Revised, Alcoa Laboratories, 1987.
17. R. MORRELL, "Handbook of Properties of Technical & Engineering Ceramics, Part 2: Data Reviews, Section 1: High-Alumina Ceramics." (HM Stationary Office, London, 1987).
18. A. WANNER, *Mater. Sci. and Engg.* **A248** (1998) 35.
19. L. C. LYNNWORTH, W. R. REA and E. P. PAPADAKIS, *J. Acoust. Soc. Am.* **70**(6) (1981) 1699.
20. J. F. NYE, "Physical Properties of Crystals" (Oxford University Press, Oxford, U.K., 1984) p. 134.
21. *Idem., ibid*. (Oxford University Press, Oxford, U.K., 1984) p. 140.
22. W. GLITZEN, (ed.), "Alumina as a Ceramic Material," Special Publ. No. 4 (The American Ceramic Society, Westerville, O. 1970).
23. R. W. RICE, in "Treatise on Materials Science and Technology," Vol. 11, edited by R. K. MacKrone (Academic Press, NY, 1977) p. 199.
24. E. A. DEAN and J. A. LOPEZ, *J. Am. Ceram. Soc.* **66** (1983) 366.
25. N. RAMAKRISHNAN and V. S. ARUNACHALAM, *Mater. Sci.* **25** (1990) 3930.
26. D. FARGEOT, C. GAULT, F. PLATON and P. BOCH, *Journal de Physique* **42** C5 (1981) 899.
27. S. PARTHASARATHI, B. R. TITTMANN, K. SAMPATH and E. J. ONESTO, *Journal of Thermal Spray Technology* **4** (1995) 367.
28. W. BRAUE, *et al*., *J. Europ. Ceram. Soc.* **16** (1996) 85.
29. M. KACHANOV, I. TSUKOV and B. SHAFIRO, *Appl. Mech. Rev.* **47**(1) (1994) S151.

Received 26 August 1999
and accepted 16 February 2000